High spin polarization in the disordered quaternary Heusler alloy FeMnVGa

Shuvankar Gupta [1,*] Sudip Chakraborty [1] Vidha Bhasin,[2] Santanu Pakhira [3] Shovan Dan [4] Celine Barreteau,[5]
Jean-Claude Crivello [5] S. N. Jha [6] Maxim Avdeev [7,8] Jean-Marc Greneche [9] D. Bhattacharyya,[2]
Eric Alleno [5] and Chandan Mazumdar[1]

[1]*Condensed Matter Physics Division, Saha Institute of Nuclear Physics, A CI of Homi Bhabha National Institute,*
1/AF, Bidhannagar, Kolkata 700064, India
[2]*Atomic & Molecular Physics Division, Bhabha Atomic Research Centre, Mumbai 400 094, India*
[3]*Ames National Laboratory, Iowa State University, Ames, Iowa 50011, USA*
[4]*Department of Condensed Matter Physics and Materials Science, Tata Institute of Fundamental Research, Mumbai 400005, India*
[5]*Univ Paris Est Creteil, CNRS, ICMPE, UMR 7182, 2 rue Henri Dunant, 94320 Thiais, France*
[6]*Beamline Development and Application Section Physics Group, Bhabha Atomic Research Centre, Mumbai 400085, India*
[7]*Australian Nuclear Science and Technology Organisation, Locked Bag 2001, Kirrawee DC, New South Wales 2232, Australia*
[8]*School of Chemistry, The University of Sydney, Sydney, New South Wales 2006, Australia*
[9]*Institut des Molécules et Matériaux du Mans, IMMM, UMR CNRS 6283, Le Mans Université, Avenue Olivier Messiaen,*
Le Mans Cedex 9, 72085, France

In this paper, we report the successful synthesis of a Fe-based highly spin-polarized quaternary Heusler alloy FeMnVGa and its structural, magnetic, and transport properties probed through different experimental methods and theoretical techniques. Density functional theory (DFT) calculations performed on different types of structures reveal that the structure with Ga at $4a$, V at $4b$, Mn at $4c$, and Fe at $4d$ (space group $F\bar{4}3m$) possess minimum energy among all the ordered variants. *Ab initio* simulations in the most stable ordered structure show that the compound is a ferromagnet having a large spin-polarization (89.9%). Neutron diffraction reveals that the compound crystallizes in disordered type-2 structure (space group $Fm\bar{3}m$) in which Ga occupies at $4a$, V $4b$ and Fe/Mn occupy $4c/4d$ sites with 50:50 proportions. The structural disorder is further confirmed by x-ray diffraction, extended x-ray absorption fine structure, ^{57}Fe Mössbauer spectrometry results, and DFT calculations. Magnetization studies suggest that the compound orders ferromagnetically below $T_C \sim 293$ K and the saturation magnetization follows the Slater-Pauling rule. Mössbauer spectrometry, along with neutron diffraction, suggest that Mn is the major contributor to the total magnetism in the compound, consistent with the theoretical calculations, which also indicates that spin polarization remains high (81.3%), even in the presence of such large atomic disorder. The robustness of the half-metallic ferromagnetic (HMF) property in the presence of disorder is a quite unique characteristic over other reported HMF in literature and makes this compound quite promising for spintronics applications.

I. INTRODUCTION

In the realm of spintronics, half-metallic ferromagnetic (HMF) materials are one of the most promising systems that can potentially generate 100% spin-polarized current due to their unusual band structure [1,2]. In such systems, one spin subband acts like a metal whereas the other subband behaves like a semiconductor [3–5]. Heusler alloys have generated a lot of interest because of their tunability among the several types of HMF materials that have been reported [6,7].

The stoichiometric representation of the Heusler alloy is X_2YZ, where X, Y are transition elements and Z is a sp-group element [7]. Recently, it was found that the quarternary variant of Heusler alloys, $XX'YZ$, have a great potential to simultaneously exhibit the spin-gapless semiconducting (SGS) [8–10]

and HMF properties, which have enormously intrigued the interest of the scientific community [11–14].

SGSs are a type of HMF in which the metallic subband only touches the Fermi level instead of complete overlapping, while the other subband remains a semiconductor [8,15]. Incidentally, most members of this subclass of Heusler alloys are found to be Co-based. Although the theoretical predictions have extended to many other Heusler alloys beyond the Co-based analogs [16,17], only a few have been experimentally realized so far, exhibiting HMF and SGS properties [9,10]. It is primarily because most of those theoretically proposed compositions were often found to be experimentally untenable to crystallize. Even those which could be formed in single phase, the majority was found to consist of multiple elements belonging to the same period of the periodic table, which is highly conducive to the cross-site occupation, resulting in significant structural disorder [7]. For example, MnCrVAl has been theoretically predicted to be a SGS when formed in a perfectly ordered crystal structure [17,18]. However, the

*guptashuvankar5@gmail.com

compounds were found to form with considerable atomic disorder and without the expected SGS characteristics. The absence of SGS behavior in this material is attributed to the site-disorder present in the actual compound [19,20]. A similar circumstance also occurs for the compound NiFeMnSn, which was theoretically predicted to be a HMF, but in the presence of large structural disorder the compound becomes metallic instead of HMF [21]. It is therefore quite logical and sensible that one has to prepare the compound as defect-free or identify the compounds where the SGS and HMF properties remain robust despite the presence of site disorder(s).

In this paper, we have extended our search for quarternary Heusler alloys beyond Co-based systems and report the synthesis and physical properties of a compound, FeMnVGa. We have determined the structural disorder using different local and bulk probes viz. Mössbauer spectrometry, extended x-ray absorption fine structure (EXAFS) and neutron diffraction. First-principles calculations in both ordered and disordered phases reveal that the spin polarization of the material is robust with respect to structural disorder. The magnetic and transport properties have also been investigated using different experimental tools.

II. METHODS

A. Experimental

The polycrystalline FeMnVGa was prepared by an arc melting procedure taking suitable high purity (>99.9%) component elements. To obtain better homogeneity, the sample was melted 5 to 6 times under argon environment and flipped after each melt. During the melting process, an extra 2% Mn was added to compensate for its evaporation. For structural characterization, both neutron and x-ray diffraction methods have been used. Powder neutron diffraction ($\lambda = 2.43$ Å) data were collected at 400 and 3 K at ECHIDNA beamline in ANSTO, Australia [22]. Cu-Kα radiation on x-ray diffractometer (model TTRAX-III, Rigaku Corp., Japan) was used to obtain powder x-ray diffraction (XRD) pattern at room temperature. The sample's single-phase nature and crystal structure were determined by performing Rietveld refinement of neutron diffraction as well as XRD data using the FULLPROF software program [23].

EXAFS measurements of the FeMnVGa samples were carried out at the Energy Scanning EXAFS beamline (BL-9) at Indus-2 Synchrotron source (2.5 GeV, 300 mA) at the Raja Ramanna Centre for Advanced Technology (RRCAT), Indore, India. The beam line operates in the photon energy range of 4–25 keV. In this beamline, a Rh/Pt-coated meridional cylindrical mirror is used for vertical collimation of the beam coming from the storage ring. The collimated beam is monochromatized by a Si (111) (2d = 6.2709 Å)-based double crystal monochromator (DCM). The second crystal of the DCM is a sagittal cylindrical crystal, which is used for horizontal focusing of the beam while another Rh/Pt coated bendable post mirror facing down is used for vertical focusing of the beam at the sample position. Rejection of higher harmonics content in the incident x-ray beam is done by detuning the second crystal of the DCM. In the present case, the measurements have been carried out in the fluorescence

mode where the sample is placed at 45 degrees to the incident x-ray beam, and a fluorescence detector is placed at right angle to the incident x-ray beam to collect the signal. One ionization chamber detector is placed prior to the sample to measure the incident flux (I_0) and florescence detector measures the fluorescence intensity (I_f). In this case, the x-ray absorption coefficient (μ) was obtained using the relation $I_T = I_0 e^{-\mu x}$, where x is the thickness of the absorber and the full absorption spectrum was obtained as a function of energy by scanning the monochromator over the specified range.

Magnetic measurements were carried out in a commercial MPMS3 (Quantum Design Inc.) in the temperature range of $3 - 380$ K and magnetic fields of up to ± 70 kOe. ^{57}Fe transmission Mössbauer spectrometry was used to investigate the atomic scale local environment and nuclear hyperfine structure of Fe. An electromagnetic transducer with a triangular velocity shape and a ^{57}Co source diffused into a Rh matrix and a bath cryostat were utilized to acquire spectra at 300 K and 77 K. The samples are made up of a thin coating of powder with a Fe content of around 5 mg Fe/cm^2. Using the in-house software MOSFIT, the hyperfine structures were simulated using a least-squares fitting approach employing quadrupolar doublets formed of Lorentzian lines. The isomer shift values were compared to those of α-Fe at 300 K, and the velocity was regulated with an α-Fe foil standard. Four-probe resistivity measurements were carried out in a commercial Physical Property Measurement System (Quantum Design Inc.).

B. Computational

Density functional theory (DFT) is used to calculate the stability and ground-state properties of the material. The projector augmented wave approach [24] included in the Vienna *Ab initio* Simulation Package was used to carry out DFT calculations [25,26]. The exchange correlation was described by the generalized gradient approximation modified by Perdew, Burke and Ernzerhof [27]. All calculations included an energy band up to a cutoff of $E = 600$ eV. The tetrahedron approach with Blöchl correction [28] was used after performing volume and ionic (for disordered structure) relaxation procedures. All calculations were done taking spin-polarization in consideration. Unit cells based on the notion of special quasi-random structure (SQS) [29] were created to model the numerous possible disorder schemes in FeMnVGa. The cluster expansion formalism for multicomponent and multisublattice systems [30], as implemented in the Monte Carlo algorithm provided in the Alloy-Theoretic Automated Toolkit [31,32], was utilized to build the SQS. Subsequently, DFT calculations were performed to see how trustworthy the DFT results are and to test the quality of the SQS. Aside from the calculations with a distinct order of interactions, the root mean square (rms) error was utilized as another quality criterion. For all clusters k, the rms error defines the departure of the SQS (Π_{SQS}^k) correlation function from the correlation function of a totally random structure (Π_{md}^k):

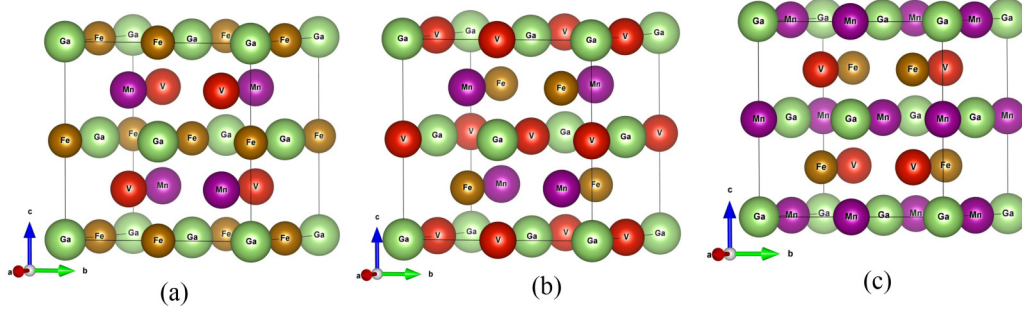$$\text{rms} = \sqrt{\sum_k \left(\Pi_{\text{SQS}}^k - \Pi_{md}^k\right)^2}. \qquad (1)$$

FIG. 1. Unit cell representation of (a) type-1 (b) type-2, and (c) type-3 ordered structures as described in Table I. Fe, Mn, V, and Ga atoms are represented by yellow, magenta, red, and green colors.

To develop the disordered structure, several tests were performed to optimize the clusters type and their numbers [Ga at $4a$ $(0,0,0)$, V at $4b$ $(0.5,0.5,0.5)$, and Fe = 0.5/Mn = 0.5 at $4c$ $(0.25,0.25,0.25)$ and Fe = 0.5/Mn = 0.5 at $4d$ $(0.75,0.75,0.75)$] from the LiMgPdSn-type crystal structure (space group F$\bar{4}$3m). Finally, to acquire reliable results, 7 pairs, 5 triplets, and 11 quadruplets interactions were considered. After several convergence tests, the SQS cell with 28 atoms (for comparison, details of SQS with many different number of atoms in the supercell are provided in Sec. I A of the Supplemental Material [33]) and a 50:50 mixing on $4c$ and $4d$ sites was considered to simulate the disordered structure.

III. RESULTS AND DISCUSSION

A. Electronic structure calculations: Ordered structure

DFT studies on FeMnVGa in LiMgPdSn-type structures (space group $F\bar{4}3m$) were first done to optimize the crystal structure and identify the most stable configuration. In a quaternary Heusler alloy $XX'YZ$, if the Z atoms are considered at position $4a$ $(0,0,0)$, the remaining three atoms X, X', and Y might be put in three alternative fcc sublattices, namely, $4b$ $(0.5,0.5,0.5)$, $4c$ $(0.25,0.25,0.25)$, and $4d$ $(0.75,0.75,0.75)$. Since the permutation of the atoms in the $4c$ and $4d$ positions leads to energetically invariant configurations, only three independent structures are viable out of a total of six potential combinations. Figure 1 depicts primitive representations of the three types of structures described in Table I. In our calculations, we took into account these three combinations, and the results are presented in Table I.

According to our calculations, the type-2 structure is the most stable arrangement. Since the shortest atomic distance is along the [111] direction, the three structure types should be first compared along this direction. Type 2 is the only

TABLE I. Calculated enthalpy of formation $\Delta_f H$ for each ordered type of FeMnVGa and one disordered case.

	$4a$	$4c$	$4b$	$4d$	$\Delta_f H$ (kJ/mol)
Type 1	Ga	Mn	Fe	V	−13.41
Type 2	Ga	Mn	V	Fe	−27.21
Type 3	Ga	V	Mn	Fe	−7.38
Disordered	Ga	Fe:Mn	V	Fe:Mn	−28.58

type that prevents Fe and Mn atoms being nearest neighbors and promotes V and Ga atoms as their nearest neighbors. Based on this result and on a recent Bader analysis on the compound Fe$_2$VAl [34], it can be surmized that V (the most electropositive atom) and Ga atoms play the role of cations whereas Fe and Mn play the role of anions in FeMnVGa. The type-2 structure, with its Ga–Mn–V–Fe sequence along [111], would be the only sequence alternating cations and anions. Total magnetic moments of full and quaternary Heusler alloy can be determined using the Slater-Pauling (S-P) rule given by $m = (N_V\text{-}24)\,\mu_B/\text{f.u.}$, where m is the total magnetic moment and N_V is the total valence electron count (VEC) [35]. Since VEC = 23 for FeMnVGa, following the convention provided by the S-P rule, the total magnetic moment should be equal to $-1\,\mu_B/\text{f.u.}$ It is crucial to note that these compounds with VEC < 24 have negative total spin moments and that the gap is situated at the spin-up band as a result of the S-P rule [36]. Additionally, contrary to the other Heusler alloys [35], the spin-up electrons correspond to the minority-spin electrons while the spin-down electrons match the majority electrons [36]. It may be pertinent to note that the negative sign of the magnetic moment used here should not be confused as a diamagnetic signature but rather due to the general convention followed by the S-P rule. Since the VEC of FeMnVGa is 23, there are 12 majority-spin electrons in the spin-down band, and 11 minority-spin electrons in the spin-up band. The negative sign on the magnetic moment here indicates that the spin-down band contains majority spins. The total magnetic moment is calculated to be $-0.93\,\mu_B$, which is quite close to $-1\,\mu_B$, as predicted by the S-P rule. The element-specific moments have also been calculated for the most stable configuration (type 2), with Fe = $-0.56\,\mu_B$, Mn = $-0.92\,\mu_B$, V = $0.53\,\mu_B$, and Ga = $0.02\,\mu_B$, resulting in ferrimagnetic structure between $z = 0$ and $z = 1/2$ layers along the c direction. It may be noted here that the relatively small magnitude of the magnetic moment in Fe as well as the nonmagnetic element, V, are the results of magnetic induction by ordered Mn moment. The predicted spin-polarized band structure and density of states (DOS) of the most energetically favorable configuration (type-2 ordered structure) are shown in Fig. 2. The minority (spin-up) band exhibits an indirect band-gap at Fermi level (E_F) while the majority (spin-down) band is metallic. The current calculations show that FeMnVGa in the type-2 structure has a very high polarization $P = \frac{\text{DOS}^\uparrow(E_F) - \text{DOS}^\downarrow(E_F)}{\text{DOS}^\uparrow(E_F) + \text{DOS}^\downarrow(E_F)} = 89.9\%$, indicating that it is a highly spin polarized ferromagnet.

(a) Majority (Spin-down) band   (b) Density of states   (a) Minority (Spin-up) band
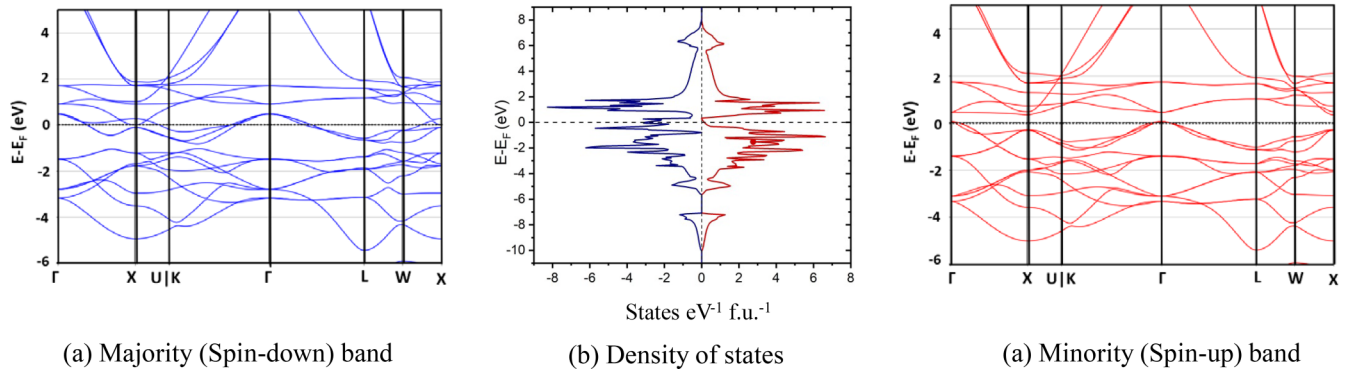
FIG. 2. Spin-polarized band structure and density of states of FeMnVGa in ordered type-2 structures: (a) majority (spin-down) band (b) density of states, (c) minority (spin-up) band. The energy axis zero point has been set at the Fermi level and the spin-up (minority) and spin-down (majority) electrons are represented by positive and negative values of the DOS, respectively.

B. Neutron diffraction

In the studied compound FeMnVGa, all the constituent atoms (Fe, Mn, V, and Ga) belong to the same period of the periodic table. For such cases in the Heusler alloy, XRD often gives delusive results about the extent of atomic disorder within the crystal structure due to the close-by x-ray scattering factors of the constituent elements. Because of its capability to distinguish nearby atoms in the periodic table whose coherent scattering amplitudes in neutron diffraction process are dramatically different, neutron diffraction is generally more sensitive to site disorder than the XRD technique [21,37,38]. The neutron diffraction pattern of FeMnVGa taken at 400 K ($T > T_C$) is presented in Fig. 3. It has already been mentioned before that one of the primary prerequisites for attaining high spin-polarization in Heusler alloys is to have a highly ordered structure since the structural disorder generally acts as a strong deterrent [39]. A2- and B2-type disorders are known to be the most frequently observed disorders in Heusler alloys. In A2-type disorder, all the constituent atoms (X, X', Y and Z) randomly mix with each other, whereas for B2-type disorder,

the Y and Z and X and X' atoms randomly mix with each other in the $4a$ and $4b$ and $4c$ and $4d$ sites, respectively [7,11]. In general, the observation of (111) and (200) superlattice peaks signifies the ordered formation of the crystal. In an A2-type disorder, both superlattice reflections are missing, whereas only the (200) peak is present in a B2-type disorder [7,40]. The structural optimization calculations discussed above have proposed that type-2 ordered structures having Ga-$4a$, V-$4b$, Mn-$4c$, and Fe-$4d$ possess minimum energy among all the probable ordered structural arrangements. However, neutron diffraction data taken at 400 K could not be explained with an ordered type-2 arrangement. Interestingly, in the neutron diffraction data taken in the paramagnetic region (400 K), the (111) peak is clearly visible, ruling the possibility of both A2- and B2-type disorders. It can thus be concluded that it is neither intermixing of all the constituent atoms (X, X', Y, and Z) in each site nor the intermixing of Y and Z and X and X' atoms, in $4a$ and $4b$ and $4c$ and $4d$ sites, respectively. However, the crystal structure cannot be identified as an ordered type-2 structure as we find the (200) Bragg peak is diffused in the neutron diffraction data, indicating the possible presence of another kind of atomic disorder. We have attempted to carry out the Rietveld refinement on the 400 K data with a disordered structure in which Ga is at $4a$, V at $4b$, and Fe/Mn with 50:50 proportions at $4c$ and $4d$ sites, respectively. Such a disordered structure presented in the Fig. 4 perfectly fits the experimental data in the paramagnetic region ($R_f = 3.83$, $R_{wp} = 5.12$) (fitting parameters for different disorder structures are provided in Sec. I B of the Supplemental Material [33]). Moreover, neutron diffraction also indicates 5% of anti-site disorder between Ga and V sites. It is very fascinating to note that the disorder between Fe/Mn enhances the symmetry of the crystal structure and the disordered structure becomes the $L2_1$ type (space group $Fm\bar{3}m$, No. 225) which is the ordered structure of ternary Heusler alloy.

C. X-ray diffraction

To determine the lattice parameter more accurately (at room temperature), we have probed the system with x-rays, using a shorter wavelength compared to neutrons. Due to Fe, Mn, V, and Ga displaying very similar atomic x-ray scattering factors, an independent structural analysis of XRD data, not
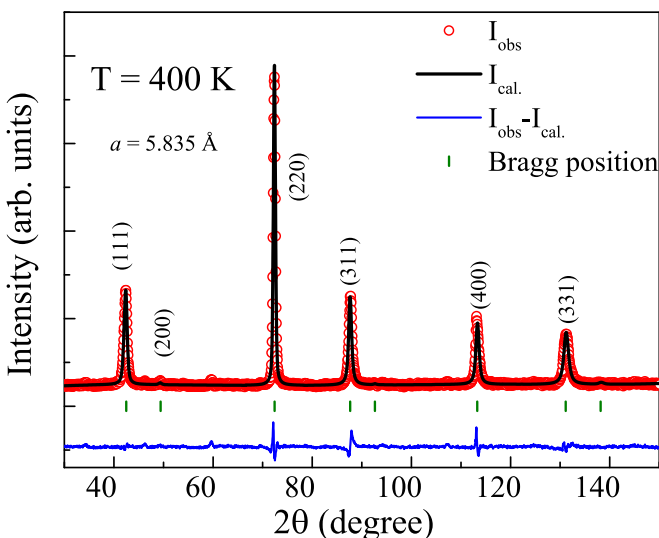

FIG. 3. Rietveld refinement of the Neutron diffraction pattern of FeMnVGa taken at 400 K.
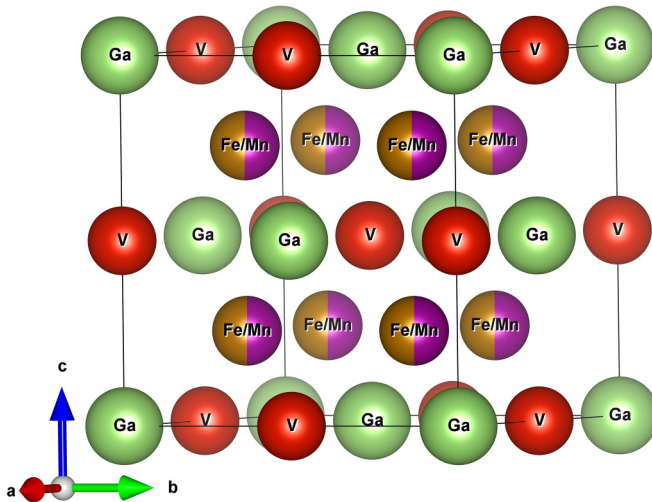
FIG. 4. Atom distribution of FeMnVGa in disordered crystal structure (L2$_1$ type, space group $Fm\bar{3}m$).

considering the structural model from neutron diffraction extracted above, could not be carried out. Any simulated x-ray patterns lead to the (111) and (200) lines being very weak or absent, making indistinguishable ordered or disordered structures [41]. In such cases, one has no other option but to rely on the structural model extracted from the neutron diffraction data analysis. Figure 5 represents the powder XRD data taken at room temperature and its Rietveld refinement, assuming the disordered structure (presented in Fig. 4) obtained from the neutron diffraction measurements. The calculated XRD pattern matches very well the experimental data (R$_f$ = 2.59, R$_{wp}$ = 3.61), showing that both diffraction experiments fully agree. The fitted lattice parameter is found to be a = 5.829 Å. It may, however, be pointed out here that the neutron diffraction and XRD pattern analysis provides only the macroscopic information on the atomic disorders. To investigate the nature
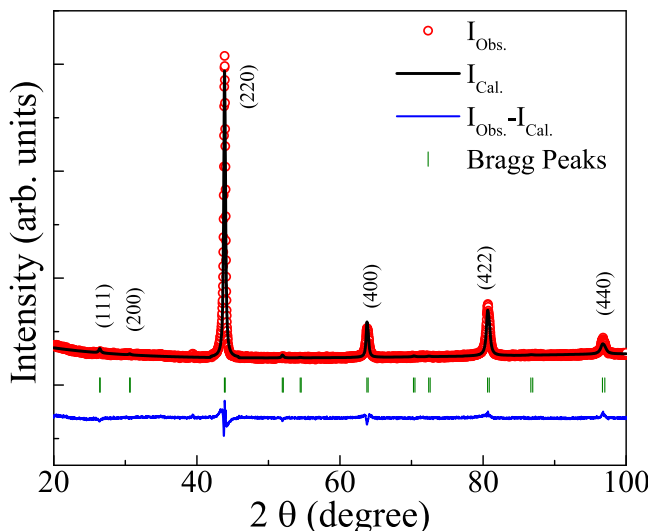

FIG. 5. Rietveld refinement of the powder XRD pattern of FeMnVGa disordered structure measured at room temperature. Miller indices of the Bragg peaks are presented in vertical first bracket.

of disorders in the local atomic environment, we have utilized the EXAFS [42–44] and ^{57}Fe Mössbauer measurements.

D. EXAFS

Unlike XRD, the EXAFS technique focuses on the atomic environment around the selected atoms. We conducted EXAFS measurements on the FeMnVGa sample at the Fe, Mn, and V edges to investigate the structural disorder in a more restricted and local scale.

Figure 6 shows the normalized EXAFS [$\mu(E)$ vs E] spectra of the FeMnVGa sample measured at Fe, Mn, and V edges. Analysis of the EXAFS data have been processed following the standard procedure [45]. In brief, to obtain quantitative information about the local structure, the absorption spectra [$\mu(E)$ vs E] have been converted to absorption function $\chi(E)$ defined as follows:

$$\chi(E) = \frac{\mu(E) - \mu_0(E)}{\Delta\mu_0(E_0)}, \tag{2}$$

where E_0 is the absorption edge energy, $\mu_0(E_0)$ is the bare atom background, and $\Delta\mu_0(E_0)$ is the absorption edge step in $\mu(E)$ value. The energy-dependent absorption coefficient $\chi(E)$ is then converted to the wave-number-dependent absorption coefficient using the relation

$$K = \sqrt{\frac{2m(E - E_0)}{\hbar^2}}, \tag{3}$$

where m is the electron mass. $\chi(k)$ is weighted by k^2 to amplify the oscillation at high k, and the $\chi(k)k^2$ functions are subsequently fourier transformed in R space to generate the $\chi(R)$ vs R plots in terms of the real distances (phase uncorrected) from the center of the absorbing atom. The ATHENA subroutine available within the DEMETER software package [46] has been used for the above data reduction including background reduction and Fourier transform. Figure 7 shows Fourier transformed EXAFS spectra [$\chi(R)$ vs R plots] of the FeMnVGa sample at Fe, Mn, and V edges.

Subsequently, the above experimental $\chi(R)$ vs R data were fitted with theoretically generated plots. The structural parameters (lattice parameters and atomic coordination numbers) acquired from the XRD/ND data have been used for theoretical modeling of the EXAFS spectra of FeMnVGa. During the fitting, bond distances (R), coordination numbers (N) (including scattering amplitudes), and disorder (Debye-Waller) factors (σ^2), which give the mean-square fluctuations in the distances, have been used as fitting parameters. In this paper, $\chi(R)$ vs R plots measured at Fe, Mn, and V edges are fitted simultaneously with common fitting parameters and for all the edges data fitting was done for a distance up to 5 Å.

The goodness of fit has been determined by the value of the R_{factor} defined by

$$R_{\text{factor}} = \frac{[\text{Im}(\chi_{\text{dat}}(r_i) - \chi_{\text{th}}(r_i))]^2 + [\text{Re}(\chi_{\text{dat}}(r_i) - \chi_{\text{th}}(r_i))]^2}{[\text{Im}(\chi_{\text{dat}}(r_i))]^2 + [\text{Re}(\chi_{\text{dat}}(r_i))]^2} \tag{4}$$

where χ_{dat} and χ_{th} refer to the experimental and theoretical values, respectively, and Im and Re refer to the imaginary and real parts of the respective quantities. The subroutines ATOMS and ARTEMIS available within the DEMETER software package [46] have been used, respectively, for the
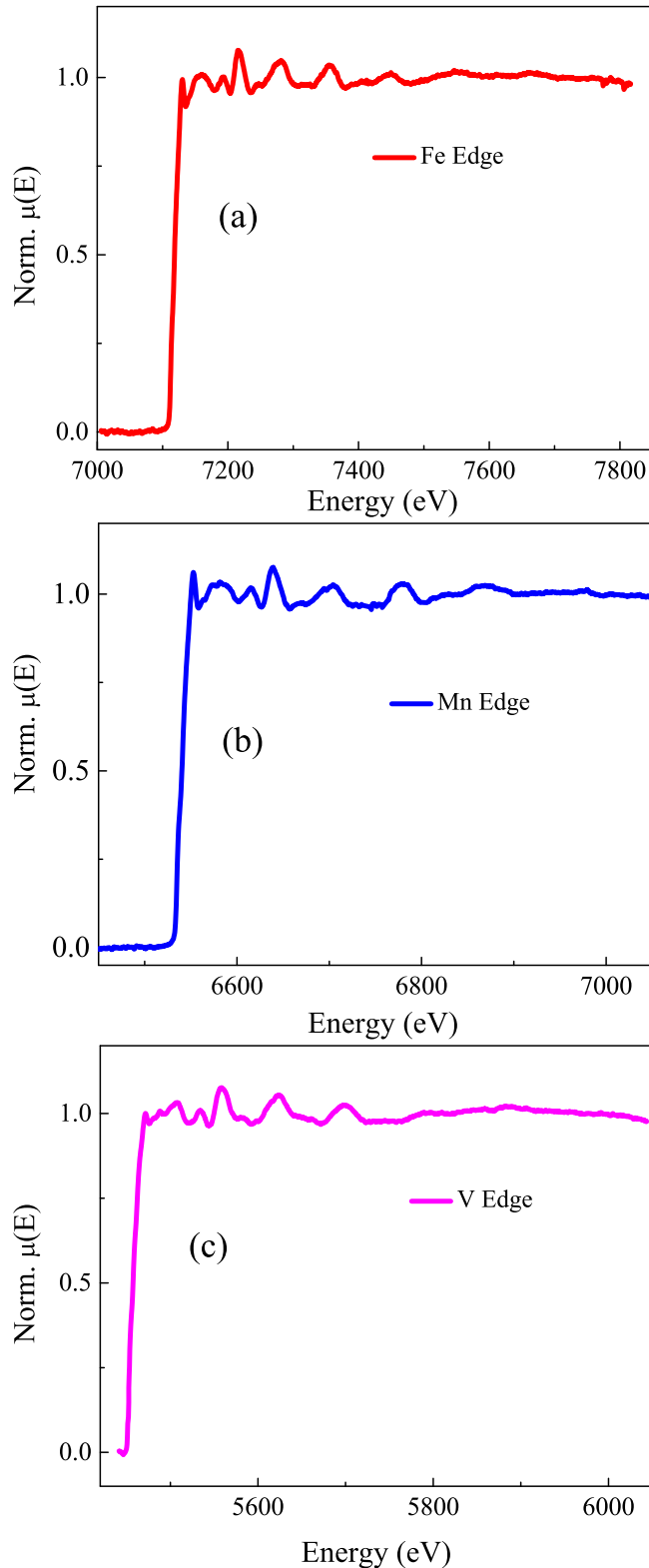
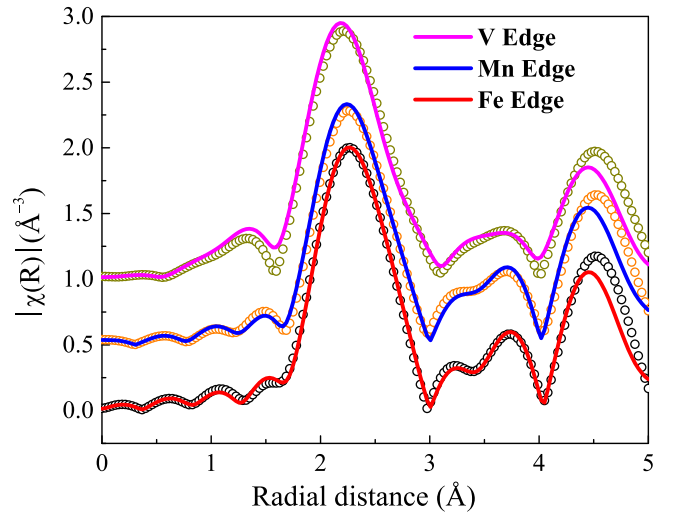FIG. 6. Normalized EXAFS spectra of FeMnVGa taken at (a) Fe edge (b) Mn edge, and (c) V edge.

FIG. 7. Fourier transformed EXAFS spectra of FeMnVGa taken at Fe, Mn, and V edges.

along with the experimental data, and the best fit parameters have been given in Table II.

It can be seen from Fig. 7 that the Fourier-transformed spectra of FeMnVGa at all three edges (Fe, Mn, V) look identical to each other, with a major peak near 2.25 Å. A similar type of EXAFS spectra was earlier observed for CoFeMnGe [43]. It is also to be noted that simultaneous fitting of all the edges (Fe, Mn, and V) is only possible assuming a disordered structure. In the Fourier transformed spectra of FeMnVGa (Fig. 7), for the Fe edge, the first major peak near 2.25 Å has contributions from Fe-Ga (2.48 Å), Fe-V (2.48 Å), Fe-Mn (2.87 Å), and Fe-Fe (2.87 Å) paths. The peak near 3.75 Å has contributions from Fe-Fe (4.06 Å) and Fe-Mn (4.24 Å) paths, while the peak near 4.50 Å has contributions from Fe-Ga (4.80 Å) and Fe-V (4.80 Å) paths. Similarly, for the Mn edge, the major peak near 2.25 Å has contributions from Mn-Ga (2.48 Å), Mn-V (2.48 Å), Mn-Fe (2.87 Å), and Mn-Mn (2.87 Å) paths, while the peak near 3.75 Å has a contribution from Mn-Mn (4.06 Å) and Mn-Fe (4.24 Å) paths. A second major peak near 4.5 Å has contributions from Mn-Ga (4.80 Å) and Mn-V (4.80 Å) paths. For the V edge, the first major peak near 2.25 Å has contributions from V-Fe (2.48 Å), V-Mn (2.48 Å), and V-Ga (2.87 Å) paths. The small peak near 3.75 Å has a contribution from V-V (4.13 Å), and the peak near 4.5 Å is due to V-Mn (4.86 Å) and V-Fe (4.86 Å) paths. We have also estimated a ratio of mixing of Fe/Mn at $4c$ and $4d$ sites from the EXAFS fitting which is found to be 50:50 from the Fe edge. Our EXAFS analysis results thus further support the presence of a disordered structure and is consistent with the neutron diffraction results (Sec. III B) and DFT calculations on the disordered structure discussed later (Sec. III H).

E. Magnetic properties

The magnetic susceptibility of FeMnVGa measured at 500 Oe under zero-field cooled (ZFC) and field cooled (FC) conditions is shown in Fig. 8. The ferromagnetic (FM)-type behavior in the magnetic susceptibility data is clearly visible, and the temperature derivative of the FC magnetic

generation of theoretical paths from the crystallographic structure and fitting of the experimental data with the theoretical simulation. Figure 7 shows the best-fit theoretical spectra

TABLE II. Bond length (R), coordination number (N), and Debye-Waller or disorder factor (σ^2) obtained by EXAFS fitting for FeMnVGa at Fe, Mn, and V edge.

Fe edge				Mn edge				V edge			
Path	R (Å)	N	σ^2	Path	R (Å)	N	σ^2	Path	R (Å)	N	σ^2
Fe-Ga	2.48 ± 0.01	4	0.0088 ± 0.0006	Mn-Ga	2.48 ± 0.01	4	0.0073 ± 0.0009	V-Fe	2.48 ± 0.01	4	0.0085 ± 0.0010
Fe-V	2.48 ± 0.01	4	0.0175 ± 0.0009	Mn-V	2.48 ± 0.01	4	0.0175 ± 0.0009	V-Mn	2.48 ± 0.01	4	0.0250 ± 0.0081
Fe-Mn	2.87 ± 0.03	3	0.0049 ± 0.0044	Mn-Fe	2.87 ± 0.01	2	0.0049 ± 0.0044	V-Ga	2.87 ± 0.01	6	0.0088 ± 0.0010
Fe-Fe	2.87 ± 0.03	3	0.0174 ± 0.0079	Mn-Mn	2.87 ± 0.01	4	0.0166 ± 0.0047	V-V	4.13 ± 0.03	12	0.0241 ± 0.0042
Fe-Fe	4.06 ± 0.03	6	0.0072 ± 0.0013	Mn-Mn	4.06 ± 0.01	6	0.0024 ± 0.0022	V-Mn	4.86 ± 0.02	12	0.0250 ± 0.0240
Fe-Mn	4.24 ± 0.03	6	0.0075 ± 0.0016	Mn-Fe	4.24 ± 0.01	6	0.0033 ± 0.0028	V-Fe	4.86 ± 0.02	12	0.0070 ± 0.0019
Fe-Ga	4.80 ± 0.03	12	0.0043 ± 0.0007	Mn-Ga	4.80 ± 0.01	12	0.0029 ± 0.0011				
Fe-V	4.80 ± 0.03	12	0.0300 ± 0.0097	Mn-V	4.80 ± 0.01	12	0.0300 ± 0.0146				

susceptibility data yielded the transition temperature of 293 K (figure not shown here). According to the S-P rule [35,47], the relationship $m = (N_V − 24)$ μ_B/f.u., where N_V is the total VEC for a material, determines the total magnetic moment (m) for Heusler alloys. The S-P rule is frequently regarded as helpful information for figuring out the link between a compound's electronic structure (the appearance of half metallicity) and its magnetism (total spin-magnetic moment). In general, the S-P rule is known to be followed by all reported Heusler-based HMFs [7,11]. For FeMnVGa, the VEC is 23, the absolute value of the S-P moment is 1 μ_B/f.u. FeMnVGa shows soft FM characteristics with little hysteresis in its isothermal magnetization, which was measured at 5 K (Fig. 9). The acquired saturation magnetization is estimated to be 0.92 μ_B/f.u, which is rather near the value anticipated by the S-P rule and DFT simulations.

F. Mössbauer spectrometry

[57]Fe Mössbauer measurements at 300 K and 77 K were carried out to obtain further insight of the structural disorder and magnetism in FeMnVGa, in relation to the Fe atom. In Fig. 10, for both the temperatures, there is just one widened and slightly asymmetrical line in the spectrum, and it is not of Lorentzian shape. Based on the Fe atom's nearly cubic symmetric surroundings, the 300 K spectrum may be explained by at least two quadrupolar doublets with tiny quadrupolar splitting values as shown in Fig. 10 and Table III. At 77 K, the spectrum is widened further and may be represented by two quadrupolar components. A slight increase in quadrupolar strength may be perceived as due to the development of a hyperfine field which is weak enough to be properly convoluted due to poor resolution. For the simplicity of analysis, the spectrum can be characterized by two components of almost equal intensity. Low values of hyperfine fields (7 kOe and 20 kOe at the two Fe sites, respectively) suggest that Fe atoms do not participate in FM ordering, indicating that the Mn moments are the primary contributor to most of the total magnetic moment. The low value of hyperfine field at the Fe sites is consistent with the induced nature of magnetic moment at the Fe-sites due to the Mn-spin ordering, as suggested in the DFT-based theoretical model on both the ordered (Sec. III A) as well as disordered structures (Sec. III H). One may note here that although Fe has just one crystallographic site in type-2 ordered structures, the existence in the
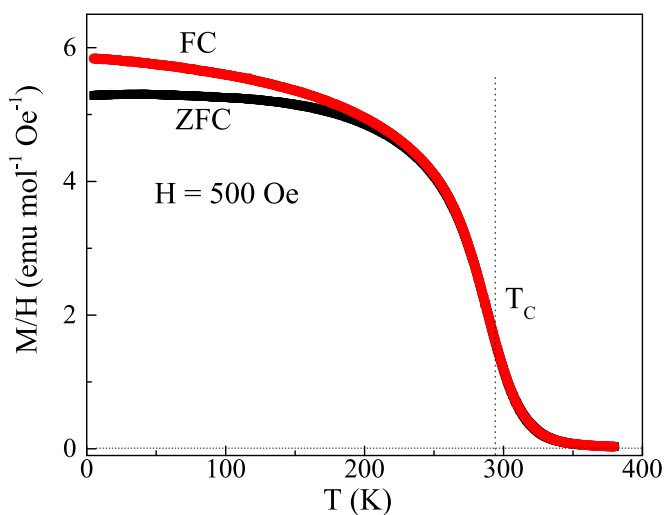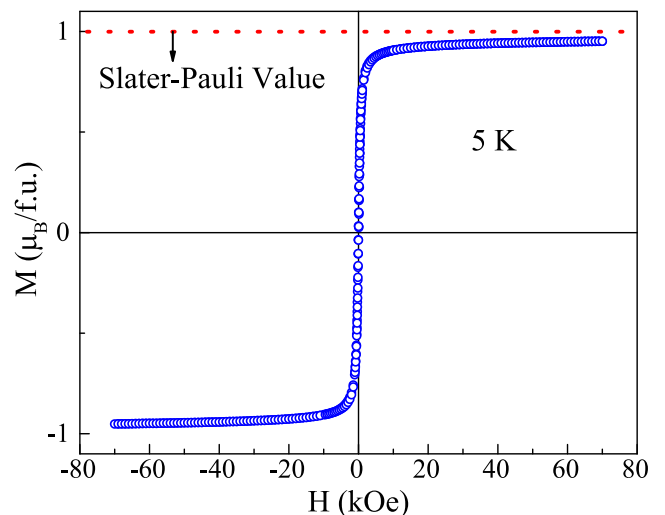

FIG. 8. Temperature dependence of magnetic susceptibility of FeMnVGa measured in a 500 Oe applied magnetic field under zero field-cooled (ZFC) and field-cooled (FC) configuration. Curie temperature, T_C, is determined from the minima in $d(M/H)/dT$ vs T plot.

FIG. 9. Isothermal magnetization of FeMnVGa measured at 5 K.
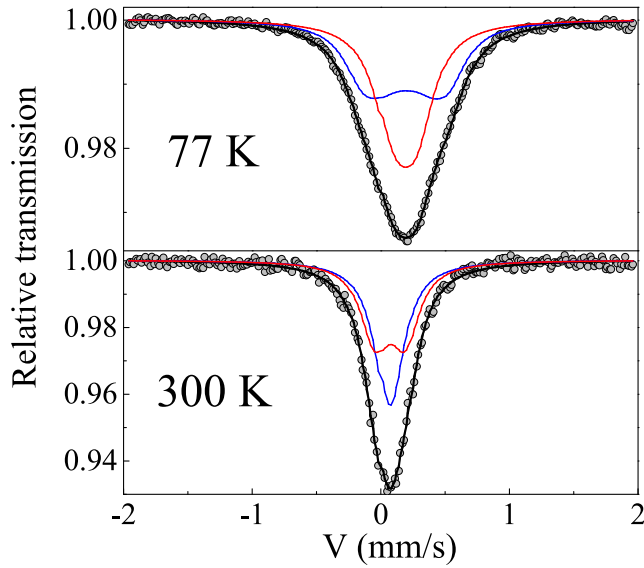
FIG. 10. Mössbauer spectra of FeMnVGa taken at (bottom) 300 K and (bottom) 77 K (top).
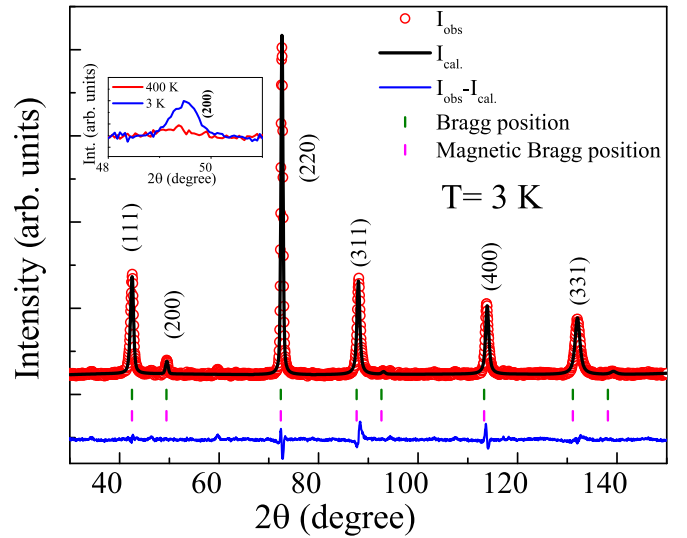

FIG. 11. Rietveld refinement of the neutron diffraction pattern of FeMnVGa taken at 3 K. The inset in (b) shows the enhancement of (200) Bragg peak intensity due to ferromagnetic ordering.

Mössbauer spectra of two components of almost equal intensities and similar hyperfine parameters suggests the availability of two locations for Fe atoms with nearly analogous structural environments. The crystal symmetry of quaternary Heusler alloy (space group $F\bar{4}3m$) is such that all the $4a$, $4b$, $4c$, and $4d$ sites correspond to tetrahedral symmetry and cannot be distinguished, leaving four options for the two Fe sites. Nonetheless, in the disordered type-2 structure where Fe and Mn randomly share the same sites (Sec. III B), the $4c$ and $4d$ sites become equivalent and the structure can then be described by space group $Fm\bar{3}m$. The $4c$ and $4d$ sites of $F\bar{4}3m$ merge into the $8c$ site of $Fm\bar{3}m$ with tetrahedral symmetry, whereas the $4a$ and $4b$ sites of the latter space group display a distinguishable octahedral symmetry. By suggesting that the two locations for Fe atoms display analogous structural environments, Mössbauer thus confirms the structural model derived from neutron diffraction. The two components are *a priori* rather equal, but the whole hyperfine structure is not well resolved, preventing a physically accurate estimation.

G. Magnetic structure

Neutron diffraction measurement in the magnetically ordered state can also help us in understanding the magnetic

TABLE III. Fitted parameter values for the Mössbauer spectra of FeMnVGa. Isomer shift (δ), line width at half height (Γ) (quoted relative to α-Fe at 300 K), quadrupolar shift ($\frac{Q}{2\varepsilon}$), hyperfine field (B_{hf}), and relative proportions (%) are estimated at 300 K and 77 K.

T (K)	Site	δ (mm/s) ± 0.01	Γ (mm/s) ± 0.01	$\frac{Q}{2\varepsilon}$ ± 0.01	$B_{hf}(T)$ ± 0.3	% ± 2
300	Fe1	0.19	0.26	0.00		50
	Fe2	0.19	0.26	0.22		50
77	Fe1	0.31	0.34	0.00	0.7	50
	Fe2	0.31	0.32	−0.01	2.0	50

spin arrangement in the system. For this purpose, we have performed the neutron diffraction experiment at 3 K and represented the data in Fig. 11, much below the magnetic transition temperature of 293 K. For antiferromagnetic (AFM) materials, below their ordering temperature, additional Bragg peaks are observed in the neutron diffraction pattern. In contrast to AFM, no additional peaks are seen in the diffraction pattern of a FM lattice, although some of the existing Bragg peaks become more intense below T_C. For FeMnVGa, a clear increase of (200) Bragg peak is overtly evident (inset of Fig. 11) which confirms the occurrence of long-range FM ordering, assuming the structural model obtained from the paramagnetic region (400 K) remain invariant. Rietveld refinement of the 3 K data was performed with an additional consideration of a magnetic structure. However, we would like to mention here that the intensity enhancement of Bragg peaks due to magnetic order is perceptible only for a single Bragg peak (200), yet the peak intensity is quite poor ($\sim$3.7% in comparison to the nuclear contribution). The enhancements of peak intensities on other Bragg peaks are even worse. Due to this limitation, the Rietveld fit gets diverged if the magnetic moment is associated with both Mn as well Fe sites or even different magnetic moments at two different Mn sites. Since the DFT calculation and ^{57}Fe Mössbauer spectra indicate very weak moments on Fe, which is of induced character, we have ignored any contribution of Fe in the neutron diffraction spectra. The contribution of ordered Mn-spins at both the $4c$ and $4d$ sites are also considered as equal. The total magnetic moment thus obtained from the Rietveld refinement of neutron diffraction data found to be 0.81(2) μ_B/f.u. for Mn atoms, which closely matches with the moment obtained from the isothermal magnetization (0.92 μ_B/f.u. measured at 5 K). The neutron diffraction measurement thus confirms that Mn is the major contributor to observed magnetism in the studied compound, consistent with the Mössbauer analysis which unveiled an absence (low value) of hyperfine field for Fe atoms (Sec. III F) and theoretical calculations (Sec. III H).

DFT calculations also estimated a site-specific moment of $0.53\,\mu_B$/f.u. for the V atoms. However, neutron diffraction discards any possibility of long-range order of V atom. The moment on the V site can be best considered as an induced moment, induced by the magnetically ordered Mn spin. Theoretical estimates of the magnetic moment often are considered as qualitative descriptions because they do not always quantitatively correlate to the empirically obtained value.

H. Electronic structure calculations: Disordered structure

When considering the crystal structure of FeMnVGa, the most plausible scenario is a disordered structure with Fe and Mn evenly distributed among $4c$ and $4d$ sites, as determined by neutron diffraction. As a result, we have revised the electronic structure analysis to account for the system's disorder. Subsequently, we find that the SQS-disordered structure's enthalpy of formation ($\Delta_f H$) is indeed lower than that of the ordered type-2 structure, with a value of -28.58 kJ/mol, i.e., the formation energy is 1.37 kJ/mol lower for the disordered structure *vis-à-vis* the ordered structure. Figure 12 represents the spin-polarized DOS of the disordered structure. The band gap is maintained by the Fermi level at the minority (spin-up) band, meaning that disordered FeMnVGa preserves its highly spin-polarized FM ground state. Despite the strong atomic disorder, the robustness of high spin polarization is evident as the spin-polarization value is changed only marginally ($P = 81.3\%$) in the disordered structure. This is due to the strange fact that disorder (between $4c$ and $4d$ sites) enhances the symmetry of the crystal structure from space group $F\bar{4}3m$ (No. 216) to space group $Fm\bar{3}m$ (No. 225), conserving the main features (highly spin polarized FM) of the electronic structure. The total magnetic contribution in the disordered structure ($-0.89\,\mu_B$/f.u.) basically remains constant in comparison to the ordered structure, as in the case of polarization. We may note that despite the distribution of Mn spins at $4c$ and $4d$ Wyckoff positions in the disordered structure, they remain not only ferromagnetically coupled but exhibit an enhanced value of $-1.2\,\mu_B$. However, the moment induced on the Fe site got reduced to $-0.21\,\mu_B$, and thus the total moment in the system ($-0.89\,\mu_B$) remains essentially unchanged *vis-à-vis* that in the ordered structure ($-0.93\,\mu_B$). It should be mentioned that we have also examined the possibility of AFM coupling of the Mn spins. However, the corresponding energy converges to the same value as that of FM coupling and further validates the FM spin arrangements of the Mn atoms.

I. Resistivity

To find the signatures of the HMF state in FeMnVGa, temperature variation of the resistivity [$\rho(T)$] was measured in the regime $5-350$ K (Fig. 13). Throughout the measurement range, the $\rho(T)$ data displays metal-like behavior. Near the magnetic transition temperature, however, a blunt change in slope was detected. The residual resistivity ratio (RRR $= \rho_{350\,K}/\rho_{5\,K}$) was estimated to be 2.45. The low value of the RRR points toward the presence of structural disorder which earlier was confirmed by Mössbauer, neutron, and EXAFS measurements [48–51]. We attempted to fit the resistivity data in the magnetically ordered state ($5 < T < 270$ K) using
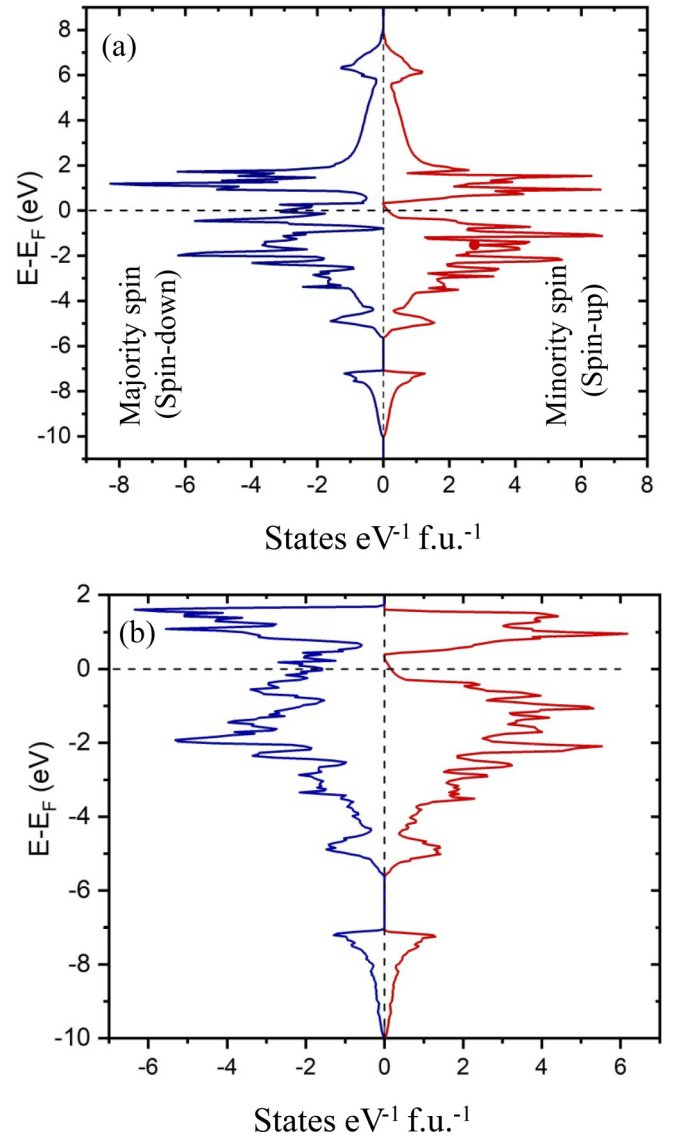

FIG. 12. (a) Density of states of FeMnVGa in ordered structures. (b) Density of states of FeMnVGa in disordered structures.

the following formula [52,53]:

$$\rho(T) = \rho_0 + A\left(\frac{T}{\Theta_D}\right)^5 \int_0^{\frac{\Theta_D}{T}} \frac{x^5}{(e^x - 1)(1 - e^{-x})} dx + BT^2,$$

(5)

where ρ_0 is the residual resistivity that arises due to lattice defects, irregularities, etc., and the second term provides the phonon scattering mechanism, in which A and Θ_D are the phonon scattering constant and Debye constant [54], respectively. The last term, BT^2, is due to magnon scattering, which remains only up to T_C [6]. It may be noted here that in most of the known HMF systems, the magnon contribution is reported to be quite small, in comparison to the phonon contribution [6,11,48]. The same is true in the present system, FeMnVGa, as well.

Equation (5), however, could not fit the experimental data well in the low temperature region $5-85$ K. Instead, low temperature ($5-85$ K) data could be well fitted using the
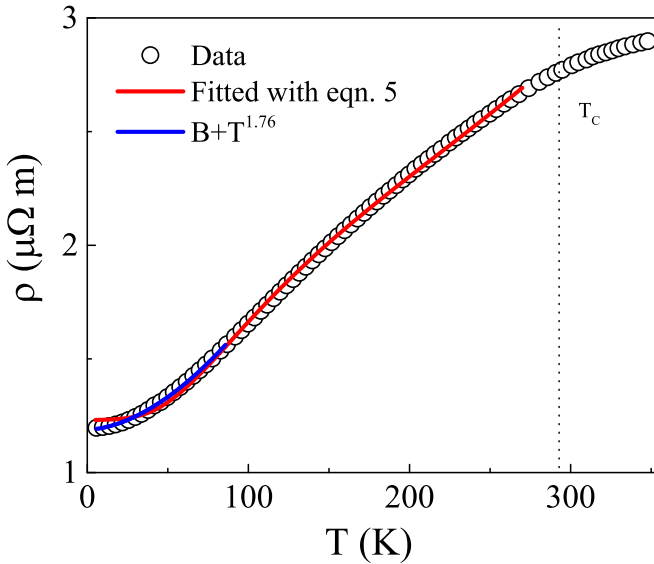
FIG. 13. Temperature dependence of the electrical resistivity measured in the absence of magnetic field in the temperature range $5 - 350$ K.

following equation,:

$$\rho = B + CT^n, \qquad (6)$$

and the value of n is found to be 1.76, which cannot be associated with any known kind of scattering. Equation (6) is widely used to fit the resistivity data for Heusler-based HMF systems in the low-temperature region. Different values of the exponent n are reported in literature in many HMF systems [48,51,55,56]. For a simple FM material, a quadratic temperature dependence of $\rho(T)$ is expected due to the magnon scattering. This value of n not equal to 2 signifies the absence of magnon scattering in the magnetically ordered region, which may look surprising at first sight. However, it is worth mentioning here that in contrast to the standard FM compounds, the HMF systems possess only one kind of band (majority or minority) at the Fermi level (E_F). The magnon contribution, which is primarily associated with spin-flip scattering, therefore may not able to contribute in a HMF system due to absence of one kind of band at E_F. Thus, our resistivity data also provide an indirect support to the presence of HMF state in FeMnVGa.

IV. CONCLUSION

In summary, we have reported here the formation of a Fe-based quaternary polycrystalline Heusler alloy FeMnVGa in a single phase using arc-melting technique. Neutron and XRD, EXAFS, ^{57}Fe Mössbauer spectrometry results, together with DFT calculation confirm that the compound crystallizes in type-2 disordered structure in which Ga is at $4a$, V at $4b$, and Fe/Mn at $4c/4d$ with 50:50 proportions. Magnetic susceptibility unambiguously exhibit FM transitions near 293 K. The saturation magnetic moment obtained from isothermal

magnetization is found to be 0.92 μ_B/f.u. which is very close to the value 1 μ_B/f.u. predicted by the S-P rule. Mössbauer spectrometry, along with neutron diffraction, suggest that Mn is the major contributor to the total magnetism in the compound consistent with the theoretical calculations. DFT calculations on the disordered structure reveal that the HMF state persists even in the disordered structure, as the spin polarization merely changes from 89.9% to 81.3% as a result of this disorder. Such robustness of HMF behavior, despite having a large crystal disorder, is rarely displayed by the Heusler alloy group of material and is quite unique over other reported HMF materials in Heusler alloys. Incidentally, such coexistence of high spin-polarization along with structural disorder have earlier been reported in a related system, FeMnVAl [57], where different sets of experiments, viz. nuclear magnetic resonance technique involving ^{27}Al and ^{51}V nuclei, along with ^{57}Fe Mössbauer spectrometry, were utilized to probe the structural disorder. In both cases, structural disorder enhances the symmetry of the crystal structure maintaining its prime feature (highly spin polarized FM) near the Fermi level. Robust half-metallicity has also been theoretically estimated for different types of site-disorders in CoFeMnSi [58], some of which even lower the crystal symmetry. Although the spin polarization remains high in most of these predicted configurations, the large band gap is, however, maintained only in the configuration where the antisite disorder involves the swapping of Co and Fe in a 50:50 ratio that improves crystal structural symmetry from $F\bar{4}3m$ to $Fm\bar{3}m$, which is also consistent with our observations. One may thus tempt to correlate the high spin polarization with disorder-induced symmetry enhancement. On the other hand, systems like MnCrVAl form with A2-type disorder [20], which happens to have higher symmetry than the ordered Y-type structure, the material lacks the theoretically anticipated SGS characteristics. Thus, it may not be possible to draw a universal rule correlating the high spin polarization with disorder-induced symmetry enhancement for any arbitrary type of disorder. Due to the introduction of structural disorder in thin films or devices based on HMFs materials, existing reported HMF exhibit very low polarization when compared to their poly-/single-crystalline mother compounds. In such cases, a compound like FeMnVGa, whose HMF property is very robust or unaffected by structural disorder, would be very useful in the preparation of thin films and devices for spintronic applications.

[1] C. Felser, G. H. Fecher, and B. Balke, Spintronics: A challenge for materials science and solid-state chemistry, Angew. Chem. Int. Ed. **46**, 668 (2007).

[2] S. A. Wolf, D. D. Awschalom, R. Buhrman, J. Daughton, S. von Molnár, M. Roukes, A. Y. Chtchelkanova, and D. Treger, Spintronics: A spin-based electronics vision for the future, Science **294**, 1488 (2001).

[3] R. A. de Groot, F. M. Mueller, P. G. van Engen, and K. H. J. Buschow, New Class of Materials: Half-Metallic Ferromagnets, Phys. Rev. Lett. **50**, 2024 (1983).

[4] J.-H. Park, E. Vescovo, H.-J. Kim, C. Kwon, R. Ramesh, and T. Venkatesan, Direct evidence for a half-metallic ferromagnet, Nature (London) **392**, 794 (1998).

[5] M. Jourdan, J. Minár, J. Braun, A. Kronenberg, S. Chadov, B. Balke, A. Gloskovskii, M. Kolbe, H.-J. Elmers, G. Schönhense *et al.*, Direct observation of half-metallicity in the Heusler compound Co_2MnSi, Nat. Commun. **5**, 3974 (2014).

[6] D. Bombor, C. G. F. Blum, O. Volkonskiy, S. Rodan, S. Wurmehl, C. Hess, and B. Büchner, Half-Metallic Ferromagnetism with Unexpectedly Small Spin Splitting in the Heusler Compound Co_2FeSi, Phys. Rev. Lett. **110**, 066601 (2013).

[7] T. Graf, C. Felser, and S. S. P. Parkin, Simple rules for the understanding of Heusler compounds, Prog. Solid State Chem. **39**, 1 (2011).

[8] S. Ouardi, G. H. Fecher, C. Felser, and J. Kübler, Realization of Spin Gapless Semiconductors: The Heusler Compound Mn_2CoAl, Phys. Rev. Lett. **110**, 100401 (2013).

[9] L. Bainsla, A. I. Mallick, M. M. Raja, A. K. Nigam, B. S. D. C. S. Varaprasad, Y. K. Takahashi, A. Alam, K. G. Suresh, and K. Hono, Spin gapless semiconducting behavior in equiatomic quaternary CoFeMnSi Heusler alloy, Phys. Rev. B **91**, 104408 (2015).

[10] L. Bainsla, A. I. Mallick, M. M. Raja, A. A. Coelho, A. K. Nigam, D. D. Johnson, A. Alam, and K. G. Suresh, Origin of spin gapless semiconductor behavior in CoFeCrGa: Theory and experiment, Phys. Rev. B **92**, 045201 (2015).

[11] L. Bainsla and K. Suresh, Equiatomic quaternary Heusler alloys: A material perspective for spintronic applications, Appl. Phys. Rev. **3**, 031101 (2016).

[12] V. Alijani, S. Ouardi, G. H. Fecher, J. Winterlik, S. S. Naghavi, X. Kozina, G. Stryganyuk, C. Felser, E. Ikenaga, Y. Yamashita *et al.*, Electronic, structural, and magnetic properties of the half-metallic ferromagnetic quaternary Heusler compounds CoFeMnZ (Z = Al, Ga, Si, Ge), Phys. Rev. B **84**, 224416 (2011).

[13] V. Alijani, J. Winterlik, G. H. Fecher, S. S. Naghavi, and C. Felser, Quaternary half-metallic Heusler ferromagnets for spintronics applications, Phys. Rev. B **83**, 184428 (2011).

[14] Y. Venkateswara, S. S. Samatham, P. D. Babu, K. G. Suresh, and A. Alam, Coexistence of spin semimetal and Weyl semimetal behavior in FeRhCrGe, Phys. Rev. B **100**, 180404(R) (2019).

[15] X. L. Wang, Proposal for a New Class of Materials: Spin Gapless Semiconductors, Phys. Rev. Lett. **100**, 156404 (2008).

[16] A. Kundu, S. Ghosh, R. Banerjee, S. Ghosh, and B. Sanyal, New quaternary half-metallic ferromagnets with large curie temperatures, Sci. Rep. **7**, 1803 (2017).

[17] Q. Gao, I. Opahle, and H. Zhang, High-throughput screening for spin-gapless semiconductors in quaternary Heusler compounds, Phys. Rev. Mater. **3**, 024410 (2019).

[18] K. Özdoğan, E. Şaşıoğlu, and I. Galanakis, Slater-Pauling behavior in LiMgPdSn-type multifunctional quaternary Heusler materials: Half-metallicity, spin-gapless and magnetic semiconductors, J. Appl. Phys. **113**, 193903 (2013).

[19] J. Herran, R. Dalal, P. Gray, P. Kharel, and P. V. Lukashev, Atomic disorder induced modification of magnetization in MnCrVAl, J. Appl. Phys. **122**, 153904 (2017).

[20] P. Kharel, J. Herran, P. Lukashev, Y. Jin, J. Waybright, S. Gilbert, B. Staten, P. Gray, S. Vallopilly, Y. Huh *et al.*, Effect of disorder on the magnetic and electronic structure of a prospective spin-gapless semiconductor MnCrVAl, AIP Adv. **7**, 056402 (2017).

[21] M. D. Mukadam, S. Roy, S. S. Meena, P. Bhatt, and S. M. Yusuf, Quantification of site disorder and its role on spin polarization in the nearly half-metallic Heusler alloy NiFeMnSn, Phys. Rev. B **94**, 214423 (2016).

[22] M. Avdeev and J. R. Hester, ECHIDNA: A decade of high-resolution neutron powder diffraction at OPAL, J. Appl. Crystallogr. **51**, 1597 (2018).

[23] J. Rodríguez-Carvajal, Recent advances in magnetic structure determination by neutron powder diffraction, Phys. B: Condens. Matter **192**, 55 (1993).

[24] P. E. Blöchl, Projector augmented-wave method, Phys. Rev. B **50**, 17953 (1994).

[25] G. Kresse and J. Hafner, *Ab initio* molecular dynamics for open-shell transition metals, Phys. Rev. B **48**, 13115 (1993).

[26] G. Kresse and J. Hafner, Norm-conserving and ultrasoft pseudopotentials for first-row and transition elements, J. Phys.: Condens. Matter **6**, 8245 (1994).

[27] J. P. Perdew, K. Burke, and M. Ernzerhof, Generalized Gradient Approximation Made Simple, Phys. Rev. Lett. **77**, 3865 (1996).

[28] P. E. Blöchl, O. Jepsen, and O. K. Andersen, Improved tetrahedron method for Brillouin-zone integrations, Phys. Rev. B **49**, 16223 (1994).

[29] A. Zunger, S.-H. Wei, L. G. Ferreira, and J. E. Bernard, Special Quasirandom Structures, Phys. Rev. Lett. **65**, 353 (1990).

[30] J. M. Sanchez, F. Ducastelle, and D. Gratias, Generalized cluster description of multicomponent systems, Phys. A: Stat. Mech. Appl. **128**, 334 (1984).

[31] A. van de Walle, Multicomponent multisublattice alloys, non-configurational entropy and other additions to the alloy theoretic automated toolkit, Calphad **33**, 266 (2009).

[32] A. van de Walle, P. Tiwary, M. De Jong, D. L. Olmsted, M. Asta, A. Dick, D. Shin, Y. Wang, L.-Q. Chen, and Z.-K. Liu, Efficient stochastic generation of special quasirandom structures, Calphad **42**, 13 (2013).

[33] See Supplemental Material at http://link.aps.org/supplemental/10.1103/PhysRevB.108.045137 for details of SQS with many different number of atoms in the supercell and Rietveld refinement fitting parameters for different disorder structures.

[34] A. Diack-Rasselio, O. Rouleau, L. Coulomb, L. Georgeton, M. Beaudhuin, J.-C. Crivello, and E. Alleno, Influence of self-substitution on the thermoelectric Fe_2VAl Heusler alloy, J. Alloys Compd. **920**, 166037 (2022).

[35] I. Galanakis, P. H. Dederichs, and N. Papanikolaou, Slater-Pauling behavior and origin of the half-metallicity of the full-Heusler alloys, Phys. Rev. B **66**, 174429 (2002).

[36] I. Galanakis, K. Özdoğan, E. Şaşıoğlu, and B. Aktaş, Doping of Mn_2VAl and Mn_2VSi Heusler alloys as a route to half-metallic antiferromagnetism, Phys. Rev. B **75**, 092407 (2007).

[37] T. Samanta, P. A. Bhobe, A. Das, A. Kumar, and A. K. Nigam, Reentrant cluster glass and stability of ferromagnetism in the Ga_2MnCo Heusler alloy, Phys. Rev. B **97**, 184421 (2018).

[38] M. P. Raphael, B. Ravel, Q. Huang, M. A. Willard, S. F. Cheng, B. N. Das, R. M. Stroud, K. M. Bussmann, J. H. Claassen, and V. G. Harris, Presence of antisite disorder and its characterization in the predicted half-metal Co_2MnSi, Phys. Rev. B **66**, 104429 (2002).

[39] Y. Miura, K. Nagao, and M. Shirai, Atomic disorder effects on half-metallicity of the full-Heusler alloys $Co_2(Cr_{1-x}Fe_x)$ Al: A first-principles study, Phys. Rev. B **69**, 144413 (2004).

[40] P. J. Webster and K. R. A. Ziebeck, Magnetic and chemical order in Heusler alloys containing cobalt and titanium, J. Phys. Chem. Solids **34**, 1647 (1973).

[41] Enamullah, Y. Venkateswara, S. Gupta, M. R. Varma, P. Singh, K. G. Suresh, and A. Alam, Electronic structure, magnetism, and antisite disorder in CoFeCrGe and CoMnCrAl quaternary Heusler alloys, Phys. Rev. B **92**, 224413 (2015).

[42] B. Balke, S. Wurmehl, G. H. Fecher, C. Felser, M. C. M. Alves, F. Bernardi, and J. Morais, Structural characterization of the Co_2FeZ (Z = Al, Si, Ga, and Ge) Heusler compounds by x-ray diffraction and extended x-ray absorption fine structure spectroscopy, Appl. Phys. Lett. **90**, 172501 (2007).

[43] L. Bainsla, A. K. Yadav, Y. Venkateswara, S. N. Jha, D. Bhattacharyya, and K. G. Suresh, Local structure studies of CoFeMnX (X = Si and Ge) Heusler alloys using x-ray absorption spectroscopy, J. Alloys Compd. **651**, 509 (2015).

[44] B. Ravel, M. P. Raphael, V. G. Harris, and Q. Huang, EXAFS and neutron diffraction study of the Heusler alloy Co_2MnSi, Phys. Rev. B **65**, 184431 (2002).

[45] D. C. Koningsberger and R. Prins, *X-Ray Absorption: Principles, Applications, Techniques of EXAFS, SEXAFS and XANES* (1987).

[46] B. Ravel and M. Newville, ATHENA, ARTEMIS, HEPHAESTUS: Data analysis for x-ray absorption spectroscopy using IFEFFIT, J. Synchrotron Radiat. **12**, 537 (2005).

[47] I. Galanakis, P. Mavropoulos, and P. H. Dederichs, Electronic structure and Slater–Pauling behaviour in half-metallic Heusler alloys calculated from first principles, J. Phys. D **39**, 765 (2006).

[48] D. Rani, Enamullah, K. G. Suresh, A. K. Yadav, S. N. Jha, D. Bhattacharyya, M. R. Varma, and A. Alam, Structural, electronic, magnetic, and transport properties of the equiatomic quaternary Heusler alloy CoRhMnGe: Theory and experiment, Phys. Rev. B **96**, 184404 (2017).

[49] J. Bœuf, C. Pfleiderer, and A. Faißt, Low-temperature properties of the semi-Heusler compound CuMnSb, Phys. Rev. B **74**, 024428 (2006).

[50] J. Nag, D. Rani, D. Singh, R. Venkatesh, B. Sahni, A. K. Yadav, S. N. Jha, D. Bhattacharyya, P. D. Babu, K. G. Suresh *et al.*, CoFeVSb: A promising candidate for spin valve and thermoelectric applications, Phys. Rev. B **105**, 144409 (2022).

[51] T. Samanta, S. Chaudhuri, S. Singh, V. Srihari, A. K. Nigam, and P. A. Bhobe, Structural, electronic, magnetic, and transport properties of the equiatomic Ni-based quaternary Heusler alloys, J. Alloys Compd. **819**, 153029 (2020).

[52] X. Gui, E. Feng, H. Cao, and R. J. Cava, Ferromagnetic Cr_4PtGa_{17}: A half-Heusler-type compound with a breathing pyrochlore lattice, J. Am. Chem. Soc. **143**, 14342 (2021).

[53] P. L. Rossiter, *The Electrical Resistivity of Metals and Alloys* (Cambridge University Press, 1991), Vol. 6.

[54] E. Grüneisen, Die abhängigkeit des elektrischen widerstandes reiner metalle von der temperatur, Ann. Phys. **408**, 530 (1933).

[55] L. Bainsla, A. Mallick, A. A. Coelho, A. Nigam, B. S. D. C. S. Varaprasad, Y. K. Takahashi, A. Alam, K. G. Suresh, and K. Hono, High spin polarization and spin splitting in equiatomic quaternary CoFeCrAl Heusler alloy, J. Magn. Magn. Mater. **394**, 82 (2015).

[56] D. Rani, L. Bainsla, K. G. Suresh, and A. Alam, Experimental and theoretical investigation on the possible half-metallic behaviour of equiatomic quaternary Heusler alloys: CoRuMnGe and CoRuVZ (Z = Al, Ga), J. Magn. Magn. Mater. **492**, 165662 (2019).

[57] S. Gupta, S. Chakraborty, S. Pakhira, C. Barreteau, J.-C. Crivello, B. Bandyopadhyay, J. M. Greneche, E. Alleno, and C. Mazumdar, Coexisting structural disorder and robust spin-polarization in half-metallic FeMnVAl, Phys. Rev. B **106**, 115148 (2022).

[58] Y. Feng, H. Chen, H. Yuan, Y. Zhou, and X. Chen, The effect of disorder on electronic and magnetic properties of quaternary Heusler alloy CoFeMnSi with LiMgPbSb-type structure, J. Magn. Magn. Mater. **378**, 7 (2015).